Dual Function of Pancreatic Endoplasmic Reticulum Kinase in Tumor Cell Growth Arrest and Survival

Aparna C. Ranganathan, Shishir Ojha, Antonis Kourtidis, Douglas S. Conklin, and Julio A. Aguirre-Ghiso

Department of Biomedical Sciences, School of Public Health and Center for Excellence in Cancer Genomics, University at Albany, State University of New York, Rensselaer, New York

Abstract

Pancreatic endoplasmic reticulum kinase (PERK)-eIF2α signaling, a component of the endoplasmic reticulum (ER) stress response, has been proposed as a therapeutic target due to its importance to cell survival in hypoxic tumors. In this study, we show that in addition to promoting survival, PERK can also suppress tumor growth of advanced carcinomas. Our results show that in squamous carcinoma T-HEp3 cells, which display low PERK-eIF2α signaling, inducible activation of an Fv2E-PERK fusion protein results in a strong G_0-G_1 arrest *in vitro*. Most importantly, Fv2E-PERK activation, in addition to promoting survival *in vitro*, inhibits T-HEp3 and SW620 colon carcinoma growth *in vivo*. Increased PERK activation is linked to enhanced p-eIF2α levels, translational repression, and a decrease in Ki67, pH 3, and cycD1/D3 levels, but not to changes in angiogenesis or apoptosis. Experimental reduction of PERK activity, or overexpression of GADD34 in a spontaneously arising *in vivo* quiescent variant of HEp3 cells that displays strong basal PERK-eIF2α activation, reverts their quiescent phenotype. We conclude that the growth-inhibitory function of PERK is preserved in tumors and upon proper reactivation can severely inhibit tumor growth through induction of quiescence. This is an important consideration in the development of PERK-based therapies, as its inhibition may facilitate the proliferation of slow-cycling or dormant tumor cells. [Cancer Res 2008;68(9):3260–8]

Introduction

An important function of the endoplasmic reticulum (ER) resident kinase pancreatic endoplasmic reticulum kinase (PERK) is to attenuate cellular protein synthesis during the unfolded protein response via phosphorylation of the α-subunit of the translation initiation factor eIF2 at Ser^{51}. eIF2 mediates the binding of the initiator tRNA ($tRNA_i^{Met}$) to the 40S ribosome during translation initiation (1). The phosphorylation of eIF2α converts it from a substrate to an inhibitor of eIF2B, its GTP exchange factor. Because the amount of eIF2B is stoichiometrically lower than eIF2α, the phosphorylation of a small pool of eIF2α is sufficient to abrogate protein synthesis (2), which allows cells to remedy the accumulation of misfolded proteins (3–6). In NIH3T3 fibroblasts and other "normal" cells, this is accomplished by PERK-dependent (*a*) activation of a stress-induced checkpoint resulting from the repression of cyclin D1 synthesis (7) and subsequent G_0-G_1 arrest and (*b*) translational up-regulation of the transcription factor ATF4, which induces genes that promote survival and adaptation to cellular stress (8, 9). Thus, activation of PERK-eIF2α pathway promotes both G_0-G_1 arrest and cell survival (7, 10). However, persistent phosphorylation of eIF2α following strong chronic ER stress can also result in apoptosis (11).

Recently, PERK activity has been shown to promote tumor growth (12). Studies on SV40-immortalized and $KiRas^{V12}$-transformed PERK mouse embryonic fibroblasts (PERK+/+ or PERK−/−), and HT29 colorectal carcinoma cells expressing dominant negative PERKΔC, showed that this pathway allows tumor cells to survive in a hypoxic environment *in vivo*. This was due to PERK-dependent translational induction of proangiogenic genes (13) as transformed cells lacking PERK or eIF2α signaling (PERK−/−, $eIF2\alpha^{S51A}$ cells) were poorly vascularized. These studies show that tumor cells can use the cytoprotective functions of PERK to support tumor growth. Other studies, however, indicate that PERK may have tumor-suppressive functions. For instance, PERK inhibition results in deregulated mammary acinar morphogenesis and hyperplastic growth *in vivo* (14). Further, ATF4 and other ER stress–activated factors mediate H-Ras–driven senescence in normal melanocytes (15). Finally, expression of a nonphosphorylatable mutant of eIF2α, or dominant-negative PKR, results in tumorigenesis of murine and human fibroblasts (16, 17). The above findings imply that activation of the PERK-eIF2α pathway could have a complex role in tumor cells; it can inhibit the cell cycle while inducing cell survival. The growth arrest function that is operational in normal cells may be especially relevant to tumors because a large proportion of tumor cells within a primary tumor as well as solitary disseminated tumor cells can be dividing slowly or be in a growth-arrested dormant/quiescent state (18–20).

We have shown that prolonged passaging in culture of highly tumorigenic human squamous carcinoma T-HEp3 cells results in the nonclonal loss of malignancy and the acquisition of a protracted dormant/quiescent phenotype upon reinoculation *in vivo* (21, 22). These cells are designated D-HEp3 and display a low extracellular signal-regulated kinase (ERK)/p38 activity ratio *in vitro*, which is reversed in T-HEp3 cells (21). Although the ERK/p38 ratio does not affect the rate of proliferation of these cells *in vitro*, the ratio is predictive of tumorigenicity or dormancy/quiescence *in vivo* (21). Furthermore, the high p38 activity in the D-HEp3 cells is responsible for increased BiP/Grp78 chaperone expression and enhanced PERK activation. These changes promote resistance to low glucose, ER stressors, and chemotherapeutic drug-induced apoptosis (23). In contrast, in T-HEp3 cells, the low p38 activity is associated with low levels of BiP/Grp78 expression,

Note: Supplementary data for this article are available at Cancer Research Online (http://cancerres.aacrjournals.org/).

Present address for A.C. Ranganathan and J.A. Aguirre-Ghiso: Division of Hematology and Oncology, Departments of Medicine and Otolaryngology, Mount Sinai School of Medicine, One Gustave L. Levy Place, New York, NY 10029.

Requests for reprints: Julio A. Aguirre-Ghiso, Division of Hematology and Oncology, Departments of Medicine and Otolaryngology, Mount Sinai School of Medicine, One Gustave L. Levy Place, Box 1079, New York, NY 10029. Phone: 212-241-8816; Fax: 212-426-4390; E-mail: julio.aguirre-ghiso@mssm.edu.

doi:10.1158/0008-5472.CAN-07-6215

PERK activation, and low stress tolerance (23). However, whether the differential activation of PERK in these HEp3 cell variants is a bystander of the ER stress status or a functional component of their growth capacity (i.e., dormant/quiescent versus tumorigenic) was unknown. The possibility that PERK might promote survival but also contribute to D-HEp3 cell quiescence made this model amenable to study how modulation of PERK signaling might regulate these distinct cellular responses in tumor cells.

Here, we show that the high basal PERK-eIF2α pathway activation in D-HEp3 cells while signaling for survival is also functionally linked to their loss of tumorigenicity. Furthermore, we show that activation of PERK and eIF2α signaling in highly malignant squamous T-HEp3 or SW620 colorectal carcinoma cells, through a dimerizable system or through pharmacologic intervention, induces not only survival but also tumor growth suppression both *in vitro* and *in vivo*. This occurs by the activation of a G_0-G_1 arrest program similar to the one observed in D-HEp3 cells.

Materials and Methods

Reagents and antibodies. AP20187 was a gift from Ariad Pharmaceuticals. Salubrinal and SB203580 were from Calbiochem. The following antibodies were from Cell Signaling: rabbit anti–p-eIF2α (Ser^{51}) and total eIF2α, anti–p-PERK (Thr^{980}), anti–p-GCN2 and total GCN2, anti–p-PKR and total PKR, anti-p53, anti-p21, anti–cleaved caspase-3, anti-cdk4, anti–phospho-histone 3 (pH3), and mouse anti–cyclin D3 and D1. Rabbit anti–cyclin A, anti–p-PERK, and total PERK (H-300) antibodies were from Santa Cruz Biotechnology. Anti–p-p38 and total p38 monoclonal antibodies were from BD Biosciences. Rabbit anti-FKBP12 was from Affinity Bioreagents. Rabbit anti-IgG1 and mouse anti-FLAG (M2) antibodies and tunicamycin were from Sigma. Anti-GADPH was from Ambion. Horseradish peroxidase–conjugated anti-mouse IgG antibody and anti-rabbit IgG antibody was from Vector Laboratories and Chemicon International, respectively.

Cell culture and generation of stable cell lines. Tumorigenic (T-HEp3) and "spontaneous" dormant (D-HEp3) human epidermoid carcinoma HEp3 cell (21), and SW620 cell lines were described previously (24). T-HEp3, D-HEp3, and SW620 cells were transduced with pBABE retrovirus encoding either β-galactosidase or Fv2E-ΔN PERK (Fv2E-PERK) as previously described (14). D-HEp3 cells were also transduced with pSHAG-MAGIC retrovirus encoding shRNAs targeting luciferase or PERK mRNAs (shPERK 1, 5′-GACCTTAACTGATGTAAGA-3′; shPERK 2, 5′-CACTTTGAACTTCGG-TATA-3′) or an empty vector control, respectively. Pools of cells stably expressing the transgene or short hairpin RNA (shRNA) were then selected using 2.5 μg/mL of puromycin. Transient transfection of pFLAG-CMV-2-GADD34 and pcDNA3.1Hygro plasmids was performed as described previously (14, 23). Proliferation and viability studies were performed as described previously (14, 23). For *in vitro* use, a 1 μmol/L ethanol stock of AP20187 was diluted in complete culture medium immediately before use. The final concentration of ethanol in the culture medium was <0.1%.

Growth of tumor cells in chick embryo and in nude mice. Cells were grown on the chorioallantoic membrane (CAM) and nude mice as described previously (21). Cells were detached with 2 mmol/L EDTA in PBS washed, and 2×10^5 to 5×10^5 cells were inoculated on the CAM of 9- to 10-d-old chick embryos (Charles River). One week postinoculation, the tumor nodules were excised, minced, and digested with collagenase, and the number of tumor cells per nodule was counted. For inoculation in nude mice, the cells were pretreated for 24 h with vehicle alone or 1 nmol/L AP20187 and 2×10^5 cells were injected s.c. into the interscapular region of 8- to 10-wk-old BALB/c nu/nu mice (Taconic Farms). The mice were given a daily injection of AP20187 i.p. at a dose of 5 mg/kg. For *in vivo* use, peritoneal injections were prepared from the 50 mg/mL ethanol stock diluted to 1.25 mg/mL in an injection solution consisting of 4% ethanol, 10% PEG-400, and 1.7% Tween in water. All injections were administered to mice within 30 min of dilution into the injection solution. When the tumors reached ~1 cm^3, the mice were euthanized.

Fluorescence-activated cell sorting analysis. To assess cell proliferation *in vitro*, cells were incubated with 10 μmol/L bromodeoxyuridine (BrdUrd) for 30 min and the incorporated BrdUrd was detected using BrdUrd flow kit (BD PharMingen) following the manufacturer's protocol. Fluorescence was quantified using an LSRII (BD PharMingen) flow cytometer as described (14, 23).

Metabolic labeling and polysome gradients. Protein synthesis was measured using [^{35}S]methionine incorporation and polysome gradient analysis as previously described (14).

Immunoblotting. Cells were washed with PBS and lysed in radioimmunoprecipitation assay buffer containing protease and phosphatase inhibitors and were then analyzed by Western blot as described previously (14, 23).

Reverse transcription-PCR analysis. GADD153 and GADD34 mRNA levels was analyzed using 1 to 2 μg of total RNA isolated from HEp3 cells (Trizol reagent, Invitrogen) using the Retroscript two-step RT-PCR kit from Ambion according to manufacturer's instructions. Glyceraldehyde-3-phosphate dehydrogenase (GAPDH) was used as loading control. Primer sequences for GADD153 were previously published (14). The following primers were used to amplify GADD34: GADD34 (F) 5′-GGCTGGTGGAAG-CAGTAAAAGG-3′; GADD34 (R) 5′-TTATCAGAAGGCTGGGAGACAGG-3′.

Immunohistochemistry. HEp3 tumors grown on CAM were excised 7 d postinoculation and frozen and embedded in optimum cutting temperature compound embedding medium. For each frozen tumor, 8.0-μm sections were cut using a cryostat and fixed in 100% ethanol, hydrated overnight, and processed for Ki67, pH3, caspase-3, and cyclin D1 staining. Briefly, the slides were rinsed in PBS and permeabilized for 10 min with 0.5% Triton X-100. The slides were then rinsed and incubated in 3% hydrogen peroxide for 20 min to block endogenous peroxidases and blocked for 1 h with normal goat serum in PBS. They were then incubated overnight at 4°C with anti-Ki67 (1:200), anti-pH3 (1:100), cycD1 (1:100), or caspase-3 (1:50) antibody or a normal IgG control followed with a biotinylated secondary antibody (Vectastain Elite ABC Kit) for 1 h at room temperature and detected using Vectastain ABC Kit following vendor's protocol. The peroxidase activity was developed by diaminobenzidine and nuclei were counterstained with hematoxylin.

Results

Divergent *in vivo* behavior of HEp3 squamous carcinoma cells differing in PERK-eIF2α signaling levels. We previously reported that D-HEp3 cells display a UPR characterized by increased chaperone expression (e.g., BiP, PDI, HSP47, and cyclophilin B) and XBP-1 splicing (23). Basal levels of p-PERK and p-eIF2α in D-HEp3 cells were higher than in T-HEp3 cells (Fig. 1*A* and *B*; ref. 23) and were enhanced by tunicamycin treatment (Fig. 1*A*). We next determined whether other eIF2α kinases were differentially regulated in D- versus T-HEp3 cells. Western blot analysis indicated that neither GCN2 (amino acid deprivation sensor; ref. 25) nor PKR (double-stranded RNA sensor; ref. 26) were differentially phosphorylated in these tumor cells (Fig. 1*C*), suggesting a correlation between p-PERK and p-eIF2α levels in D- versus T-HEp3 cells. Analysis of *in vitro* protein synthesis revealed that T-HEp3 cells have elevated levels of polysomes relative to D-HEp3 cells (Fig. 1*D*). Thus, the high levels of PERK-eIF2α signaling and reduced translation initiation in the D-HEp3 cells may be linked to their *in vivo* quiescent phenotype and to an unexpected growth-inhibitory function in tumor cells.

Inducible activation of PERK in malignant T-HEp3 cells causes growth arrest and survival but not apoptosis *in vitro*. To determine whether increasing PERK activity in T-HEp3 cells could mimic the quiescent phenotype of D-HEp3 cells, we expressed an Fv2E-ΔNPERK construct (Fv2E-PERK), where the Fv2E dimerization domain is fused to the cytoplasmic kinase domain of PERK (27). Because it lacks the ER luminal domain,

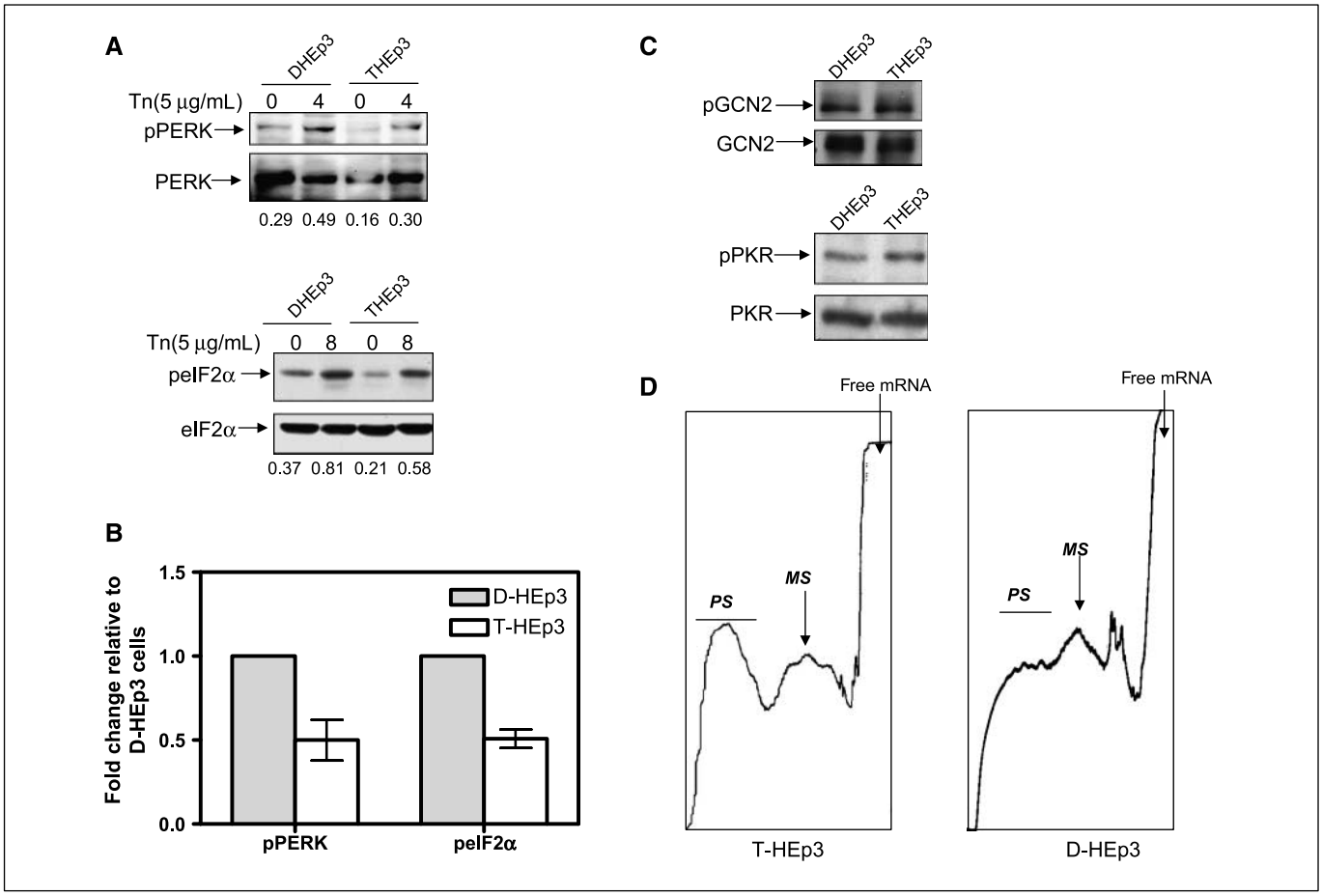

Figure 1. Analysis of basal levels of PERK and eIF2α phosphorylation and translation initiation. *A,* T- and D-HEp3 cells were treated for the indicated time points with 5 μg/mL tunicamycin and were analyzed by Western blot for phospho-Thr^{980}-PERK (*top*) and for phospho-Ser^{51}-eIF2α (*bottom*). Total PERK and total eIF2α levels served as the respective loading controls. The numbers on bottom of each lane indicate the normalized p-PERK/PERK and p-eIF2α/eIF2α absorbance for each band. *B, columns,* mean fold change (n = 3) in normalized p-PERK and p-eIF2α levels relative to D-HEp3 cells; *bars,* SE. *C,* Western blot analysis of lysates from the indicated cells for p-GCN2 (*top*) and p-PKR (*bottom*). Total GCN2 and total PKR were used as loading control. *D,* polysome gradient analysis of T- and D-HEp3 cytoplasmic lysates fractionated by sucrose density ultracentrifugation. The position of the free mRNA and the polysome (*PS*) and monosome (*MS*) peaks are indicated. The increase in the monosome peak and a decrease in the polysome peak in D-HEp3 cells relative to T-HEp3 cells are indicative of translation attenuation.

Fv2E-PERK does not respond to ER stress but can only be activated in the presence of the dimerizing drug AP20187. This allowed us to test the effect of PERK signaling independently of other ER stress pathways (i.e., XBP-1, ATF6, and GCN2). Treatment of T-Fv2E-PERK cells with AP20187 (1 nmol/L) resulted in the activation of Fv2E-PERK as detected using anti–p-PERK antibody (Fig. 2*A, top*) or anti-FKBP antibody, which detects both the hypophosphorylated and hyperphosphorylated forms of Fv2E-PERK (Fig. 2*A, bottom*). Although the levels of hyperphosphorylated Fv2E-PERK remain constant throughout the course of the treatment (Fig. 2*A, bottom*), the levels of p-PERK (Thr^{980}), which is one measure of active PERK, increases in a time-dependent manner (Fig. 2*A, top*). The difference in the phosphorylation status of Fv2E-PERK as measured with anti–Thr-980 and anti-FKBP antibody may be attributed to the phosphorylation of other residues on PERK (28, 29). Phosphorylation of endogenous eIF2α was detected as early as 2 h and was sustained for up to 8 h (Fig. 2*B, top*). By 24 h, it was completely abolished despite persistent PERK activation. The downstream target genes *CHOP* (transcription factor) and *GADD34* (regulatory subunit of the eIF2α phosphatase PP1C) were induced within 2 h following drug treatment (Fig. 2*B, bottom*) and the decrease in p-eIF2α levels at 24 h may be due to enhanced phosphatase activity as it correlated with increased *GADD34* mRNA levels. Treatment with AP20187 had no effect on pathway activation in vector (β-gal) control cells (Fig. 2*A* and *B* and data not shown). Similar to the high PERK signaling in D-HEp3 cells, Fv2E-PERK activation in T-HEp3 cells also conferred resistance to glucose deprivation (Supplementary Fig. S1*A*; ref. 23). Additionally within 2 h following Fv2E-PERK activation in T-HEp3 cells, there was a significant decrease in protein synthesis as measured by [^{35}S]methionine incorporation into newly synthesized proteins (Fig. 2*C*). These results show that Fv2E-PERK activates a pathway and cellular responses similar to that of endogenous PERK.

We found that activation of Fv2E-PERK caused a significant reduction in tumor cell proliferation as revealed by a decrease in cells in S-phase and a corresponding increase in cells in G_0-G_1 24 to 48 h following AP20187 treatment. Importantly, there was no significant increase in sub-G_0/apoptotic phase (Fig. 2*D*), suggesting that Fv2E-PERK activation does not induce general cellular toxicity in this system. Treatment with higher AP20187 concentrations (4–10 nmol/L and 1–4 μmol/L) also resulted in growth arrest with no effect on apoptosis (Supplementary Fig. S1*B* and data not shown). However, the growth arrest was reversible as early as 24 h following washout of the drug (data not shown), suggesting

that continuous treatment with AP20187 maybe required to maintain Fv2E-PERK activation and a prolonged arrest. Accordingly, we found that a daily treatment with 1 nmol/L AP20187 was able to sustain growth arrest for up to 5 days *in vitro* without any effect on cell viability (data not shown). We conclude that activation of the PERK-eIF2α pathway in the T-HEp3 cells results in concomitant growth arrest and survival programs, but not apoptosis.

Inducible activation of PERK suppresses tumor growth of T-HEp3 cells. The above findings reveal that the growth-inhibitory function of PERK in normal cells can also be invoked in tumor cells. Thus, we next tested whether the Fv2E-PERK–mediated growth arrest *in vitro* would also result in reduced tumor growth *in vivo*. To test this, Fv2E-PERK–expressing cells, which were pretreated in culture with 1 nmol/L AP20187 for 24 h, were inoculated s.c. in nude mice (0.2×10^6 cells) and treated once daily i.p. with vehicle alone or with AP20187 (5 mg/kg) for up to 40 days. Vehicle-treated mice developed palpable tumors ~10 days postinoculation and went on to form rapidly growing tumor masses that reached ~1,000 mm^3 (Fig. 3*A*). In striking contrast, and as predicted from our *in vitro* experiments, mice treated with AP20187 did not develop tumors throughout the course of the treatment (Fig. 3*A*). Tumor growth in mice injected with T-β-Gal cells was unaffected by AP20187 treatment at the same doses (Supplementary Fig. S1*C*). We next tested whether the tumor growth inhibition by 5 mg/kg of AP20187 for 16 or 20 days was reversible. Interruption of AP20187 treatment did not result in tumor growth although viable tumor cells were still present (as

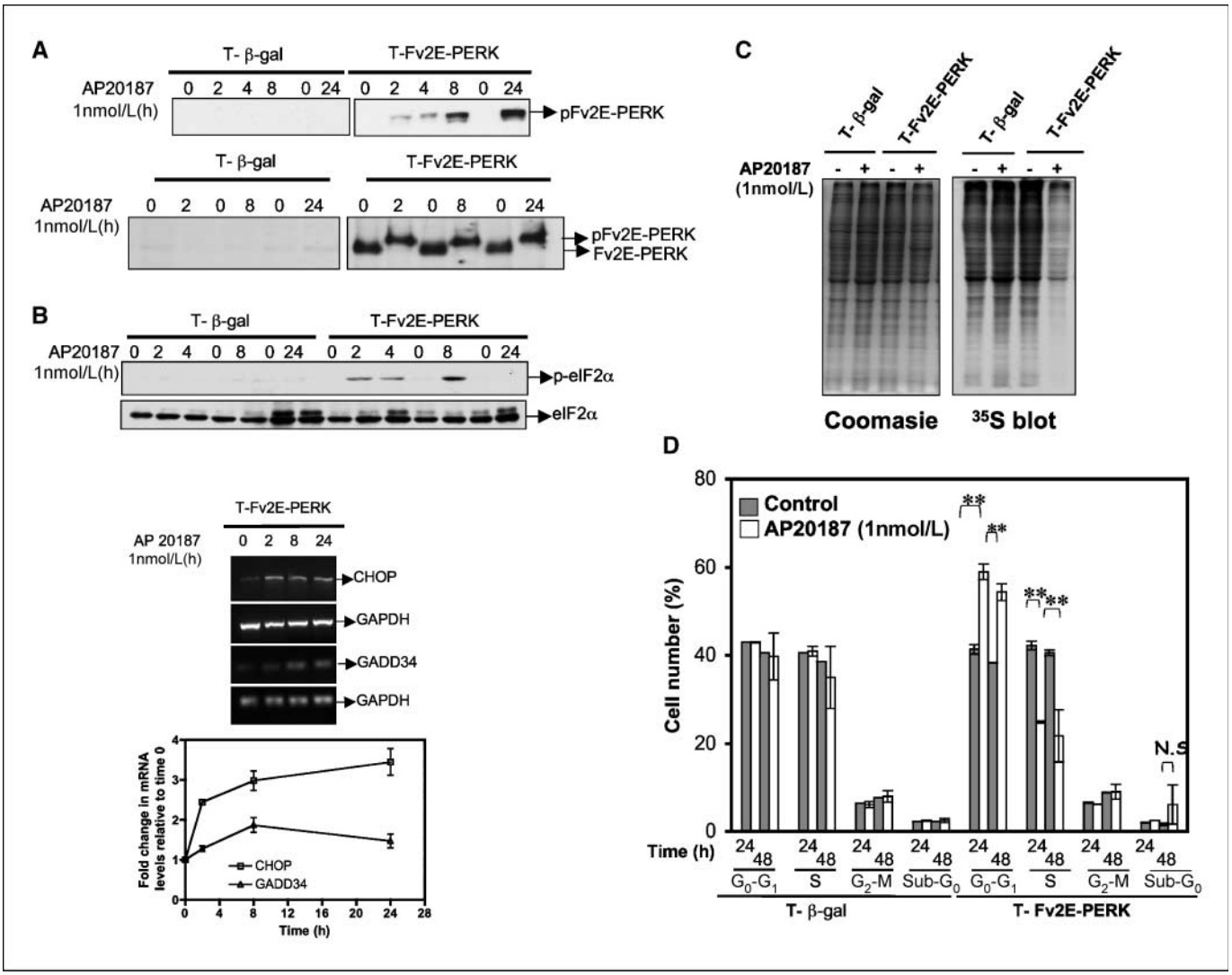

Figure 2. Inducible activation of Fv2E-PERK in T-HEp3 cells. *A,* immunoblot of time-dependent activation of Fv2E-PERK following treatment with 1 nmol/L AP20187 (AP) was measured using an anti–p-PERK (Thr^{980}) antibody that is specific for mouse as Fv2E-PERK is derived from mouse origin (*top*) and an anti-FKBP antibody that detects both the active phosphorylated and inactive hypophosphorylated Fv2E-PERK (*bottom*). *B,* lysates and RNA of T-HEp3 cells expressing Fv2E-PERK or β-gal, respectively, treated with AP (1 nmol/L) for the indicated times were analyzed by Western blot for p-eIF2α levels (*top*) and by RT-PCR for its downstream targets CHOP and GADD34 (*middle*). Total eF2α protein and GAPDH mRNA levels were used as loading controls. *Points,* average of CHOP and GADD34 mRNA levels normalized to GAPDH at each time point were quantified and expressed as fold change relative to time 0 (*bottom*); *bars,* SE. *C,* autoradiogram of [^{35}S]methionine incorporation (*right*) into newly synthesized proteins in Fv2E-PERK or β-gal–expressing T HEp3 cells that had been left untreated or treated with 1 nmol/L AP20187 for 2 h. Coomassie blue staining of the same gel indicates equal loading (*left*). *D,* cell cycle analysis of T-HEp3 cells expressing Fv2E-PERK or β-gal following treatment with 1 nmol/L AP20187 for the indicated time points. DNA synthesis was assayed by incorporation of BrdUrd and cell cycle was analyzed by uptake of 7-amino-actinomycin D and assayed by flow cytometry. Percentage of cells in the different phases were calculated using BD FACSDiva software, excluding aggregates. *Columns,* mean of three independent experiments done in duplicate; *bars,* SD. **, $P < 0.001$ as determined by paired Student's *t* test.

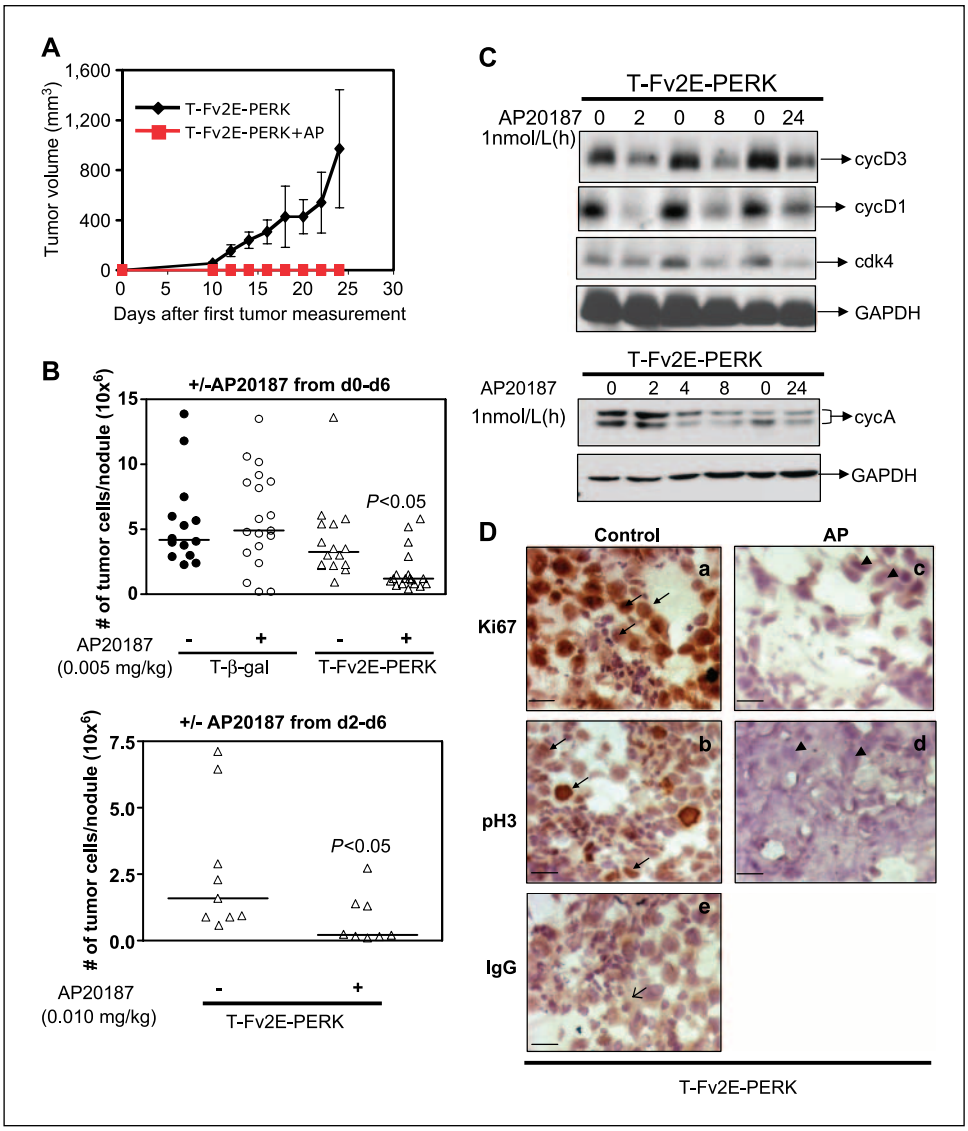

Figure 3. Activation of Fv2E-PERK inhibits tumor growth *in vivo*. *A,* T-Fv2E-PERK cells pretreated with 1 nmol/L AP20187 for 24 h and 0.2 × 10^6 cells were inoculated s.c. into the interscapular region as described in Materials and Methods. Postinoculation, mice were injected daily i.p. with AP20187 (5 mg/kg) and monitored every other day for tumor take. When tumors were detected, tumor diameter was measured and the volume was calculated and plotted as described in Materials and Methods. *B, top,* T-β-gal or T-Fv2E-PERK cells (0.2 × 10^6/CAM) were inoculated on CAMs in the presence of AP20187 or vehicle alone. The cells were treated daily with AP20187 and 7 d postinoculation, tumors were excised and the number of tumor cells per nodule was counted. *Bottom,* T-Fv2E-PERK cells were inoculated on CAM; 2 d postinoculation, cells were treated with either vehicle alone or with AP20187 at the indicated dose for 5 d. Seven days postinoculation, tumors were excised and quantified as above. *Line,* median. $P < 0.05$, Mann-Whitney test. *C,* lysates of T-Fv2E-PERK cells treated with or without 1 nmol/L AP20187 for 24 h were immunoblotted for cycD1, cycD3, and cdk4 (*top*) and cycA (*bottom*). GAPDH was used as loading control. *D,* tumor nodules from Fv2E-PERK–expressing cells treated with or without AP20187 were excised 7 d postinoculation and fixed and prepared for histologic examination (see Materials and Methods). Tumor sections from control (*a*) and AP20187-treated (*c*) CAMs were stained with the proliferation marker Ki67. Tumor cells can be distinguished from the chicken CAM cells by their size and large nuclei (*arrowheads*); *arrows,* brown staining of the nuclei generated by the Ki67 detection. *b* to *d,* staining of tumor sections with another proliferation marker pH3 (*arrow,* brown nuclear stain). Note the varying intensity of the Ki67 and pH3 staining in the control tumors and the lack of staining in the AP20187-treated tumors. *e,* T-Fv2E-PERK–derived tumor sections stained with a isotype-matched IgG; *open arrow,* the lack of staining in the nuclei and a light background staining of the cytoplasm. *Scale bar,* 40 μm.

measured by trypan blue, data not shown) in 37.5% (n = 8) of the mice in which we could find residual lesions after examining the inoculum site. These residual T-Fv2E-PERK cells (see Materials and Methods) failed to proliferate in culture (data not shown). This suggests that this level of PERK activation in T-HEp3 cells induces a context-dependent (*in vivo*) irreversible growth arrest. In experiments where lower doses (3 mg/kg) of AP20187 were used, some tumors were able to resume growth after a latency of 30 days, suggesting that it is a dose-dependent effect (data not shown).

To better understand how PERK reactivation might affect early steps of tumor cell proliferation *in vivo*, we took advantage of the chicken embryo CAM system, which allows us to quantify tumor cell proliferation *in vivo* during the 1st week of tumor growth (30). Moreover, because the chicken embryo CAM is highly vascularized (30), early tumor growth is not completely dependent on neovascularization. T-β-gal– and T-Fv2E-PERK–expressing cells were inoculated *in vivo* on the CAMs of embryonic day 9 or day 10 chicken embryos with or without 0.005 mg/kg AP20187, which is the lowest dose suggested for *in vivo* use. The treatment was

continued daily for the next 7 days. We found that the vehicle-treated cells formed large tumors and underwent five to seven cell divisions in 7 days similar to the parental T-HEp3 cells. In contrast, treatment with AP20187 resulted in a 3-fold decrease in the number of T- Fv2E-PERK tumor cells per nodule (Fig. 3*B, top*) whereas T-β-gal cells were unaffected by the treatment. Alternatively, enhancement of p-eIF2α levels using a pharmacologic inhibitor (Salubrinal) of GADD34 also resulted in a significant suppression of T-HEp3 tumor growth (Supplementary Fig. S3). Together, these results suggest that PERK activation in T-HEp3 cells suppresses tumor growth, which is more likely associated with a growth arrest as revealed by the *in vitro* studies.

We next investigated whether activating PERK signaling in already proliferating tumor cells *in vivo* is sufficient to inhibit tumor growth. T-Fv2E-PERK cells were inoculated on CAM. Two days postinoculation, a time point at which cells are actively proliferating (31), the cells were treated daily for 5 days with 0.010 mg/kg of AP20187. This treatment was also able to suppress the tumor growth by 2- to 3-fold (Fig. 3*B, bottom*). In nude mice inoculated with T-Fv2E-PERK cells, starting the treatment with AP20187 (5 mg/kg) when mice already had palpable tumor nodules also resulted in extended latency, reduced growth rate, or even complete suppression of tumor growth (Supplementary Results; Supplementary Fig. S1*E* and S1*F*). A single pretreatment of T-Fv2E-PERK cells with AP20187 *in vitro* was also sufficient to delay tumor cell proliferation *in vivo* (Supplementary Fig. S1*D*). The above results suggest that enhancement of PERK-eIF2α signaling can suppress tumor growth even of already growing T-HEp3 tumors.

SW620 cells, a highly tumorigenic and metastatic cell line (32, 33), also display low levels of p-eIF2α when compared with D-HEp3 cells (Fig. 4*A, left*). Activation of Fv2E-PERK in these cells also resulted in an increase in p-eIF2α levels (Fig. 4*A* and *B*) and a 3-fold decrease in tumor growth compared with vector control cells (Fig. 4*D*). These results strongly suggest that activation of PERK causing inhibition of tumor growth is not limited to T-HEp3 cells but is also observed in other tumor cells.

Fv2E-PERK–mediated growth suppression in T-HEp3 cells is due to decreased proliferation and not enhanced apoptosis. PERK activation was shown to promote growth arrest of normal cells by specifically inhibiting cyclin D1 synthesis (7, 10). Thus, we measured cyclin D1 levels in T-Fv2E-PERK cells following AP20187 treatment *in vitro*. Within 2 h following PERK activation, there was a significant decrease in the cycD1 protein levels that was sustained up to 24 hours. The levels of other cell cycle regulators cycD3, cdk4, cdk6, and cycA were also concomitantly down-regulated following PERK activation (Fig. 3*C*; Supplementary Fig. S2*A* and data not shown). This inhibition seemed to be specific as other cell cycle regulators such as p53 and p21 were unaffected by PERK activation (Supplementary Fig. S2*A* and data not shown). Also, the levels of phospho-p38 or total p38 and ERK were unaffected following PERK activation (Supplementary Fig. S2*A*), suggesting that a PERK-mediated inhibition of these cyclins and cyclin-dependent kinases is independent of these pathways. A similar decrease in cyclin D1 levels was also observed in SW-Fv2E-PERK cells at 24 h (Fig. 4*C*). We cannot rule out the possibility that additional mechanisms involving the regulation of

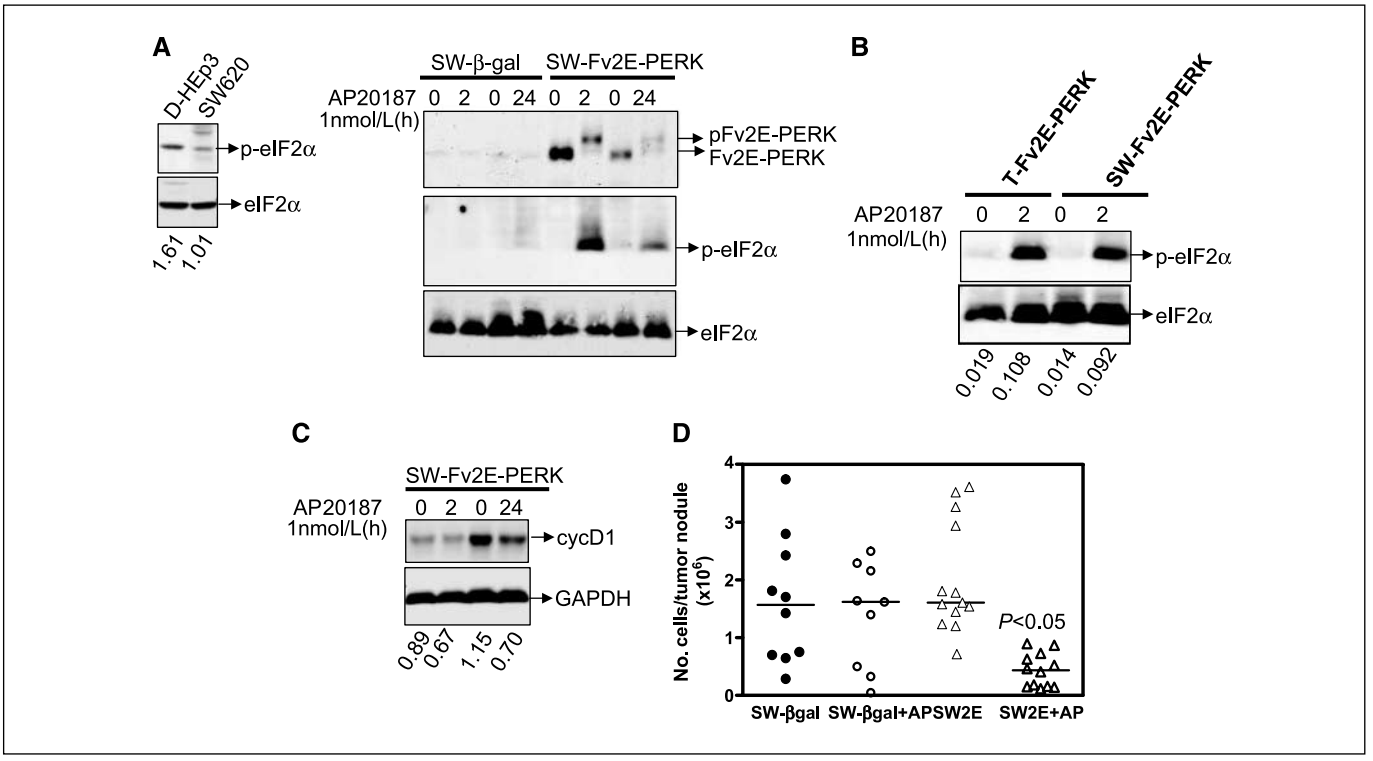

Figure 4. Activation of Fv2E-PERK inhibits tumor growth of SW620 colon carcinoma cells. *A,* Western blot analysis of D-HEp3 and SW620 lysates for p-eIF2α and total eIF2α, respectively (*left*). Vehicle and AP20187 (1 nmol/L)–treated lysates of SW620 cells expressing β-gal or Fv2E-PERK, respectively, were analyzed for active phosphorylated and inactive hypophosphorylated Fv2E-PERK and p-eIF2α levels, respectively. Total eIF2α was used as a loading control (*right*). *B,* T-Fv2E-PERK and SW-Fv2E-PERK cells treated with or without AP20187 were analyzed for p-eIF2α and total-eIF2α levels by Western blot. *C,* SW-Fv2E-PERK cells were treated with AP20187 for the indicated time points and analyzed by Western blot for cyclin D1 levels. GAPDH was used as loading control. *D,* SW620 cells expressing β-gal or Fv2E-PERK were inoculated on CAM at 0.5×10^6/CAM and treated daily with vehicle alone or with 0.005 mg/kg of AP20187. Tumors were excised 7 d later and the number of tumor cells per nodule was determined as before. $P < 0.05$ as determined by Mann-Whitney test.

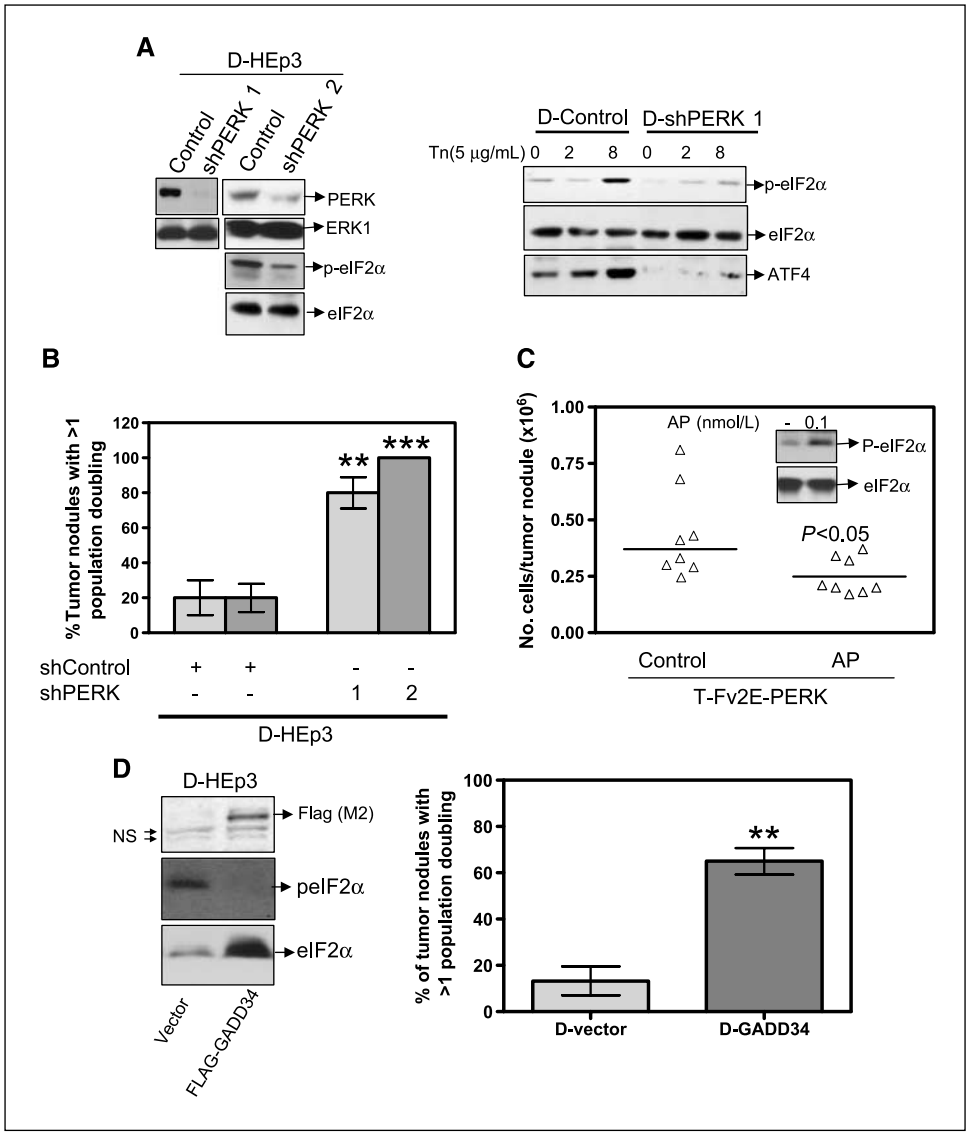

Figure 5. PERK activation contributes to the dormancy program of D-HEp3 cells. *A,* immunoblot analysis of lysates from D-control and D-shPERK–expressing cells for PERK (*left*), p-eIF2α (*left* and *right*), and ATF4 levels (*right*). ERK1 and total eIF2α serve as loading control. *B,* D-HEp3 cells infected with a control vector or shPERK were inoculated onto CAM at 0.4×10^6 to 1.0×10^6 cells/CAM. Seven days later, the number of tumor cells per nodule was quantified and the tumor population divisions were estimated. *Columns,* average of the percentage of tumor nodules with >1 population division; *bars,* SE. *** and **, $P < 0.05$ as determined by Mann-Whitney test. Passaging *in vivo* of the control cells did not form progressively growing tumors despite having undergone, in some cases, >2 population doublings. *C,* T-Fv2E-PERK cells were pretreated with 0.1 nmol/L AP20187 for 24 h and then 0.2×10^6 cells were inoculated in the presence or absence of AP20187 (5×10^{-4} mg/kg) for 4 d. Tumors were then excised and the number of tumor cells per nodule was quantified. *Line,* median. $P < 0.05$ as determined by Mann-Whitney test. *Inset,* immunoblot showing the levels of p-eIF2α in T-Fv2E-PERK cells treated with 0.1 μmol/L AP20187 for 2 h. Total eIF2 served as a loading control. *D,* D-HEp3 cells were transiently transfected with a control vector or cDNA encoding FLAG-tagged GADD34. Twenty-four hours posttransfection, a fraction of the cells was lysed and immunoblotted with anti-FLAG, anti–p-eIF2α, and anti–total eIF2α antibodies, respectively (*left*). The remaining cells were inoculated onto CAM at 0.5×10^6/CAM (*right*). **, $P < 0.05$, as determined by Mann-Whitney test.

cdk2 activity may also be at work, because cycD1 decrease was not absolute.

We then determined whether tumor growth inhibition *in vivo* was due to decreased proliferation or increased apoptosis. Frozen sections from control and AP20187 treated T-Fv2E-PERK tumors were analyzed by immunohistochemistry for proliferation markers Ki67, pH3, and an apoptosis marker, cleaved caspase-3. Tumor sections from both control and AP20187-treated tumors had similar (~5%) levels of caspase-3 staining (Supplementary Fig. S2*B*). Control Fv2E-PERK tumors stained positive for both Ki67 and pH3 (Fig. 3*D*). In sharp contrast, AP20187-treated Fv2E-PERK tumors were negative for both Ki67 and pH3, respectively, indicating growth arrest. The percentage of cells positive for cycD1 were also 3- to 4-fold lower in the AP20187 treated nodules compared with untreated control tumors (Supplementary Fig. S2*B*). Furthermore, we found no difference in the vascular density of either control or AP20187-treated T-Fv2E-PERK tumors (Supplementary Fig. S2*C*). To summarize, both our *in vitro* and *in vivo* findings strongly suggest that the growth suppression observed following PERK activation is a direct consequence of decreased proliferation and not a result of enhanced apoptosis or decreased angiogenesis.

High endogenous PERK-eIF2α signaling in D-HEp3 cells contributes to the quiescence program *in vivo*. Our above results indicate that activation of PERK-eIF2α signaling could function to suppress tumorigenesis through growth arrest. Accordingly, we determined whether the high basal levels of PERK activity in D-HEp3 cells is functionally responsible for their *in vivo* growth arrest program. D-HEp3 cells were virally infected with a vector encoding two shRNAs to PERK (shPERK 1 or shPERK 2) or to luciferase or an empty vector (D-control). Western blot analysis showed that, compared with the vector control cells, the expression of either shRNA resulted in a significant reduction in total PERK protein levels (Fig. 5*A*). This down-regulation was accompanied by a decrease in basal and tunicamycin-induced levels of p-eIF2α (Fig. 5*A*). As reported (11), this reduction in p-eIF2α levels did not increase ^{35}S-protein labeling (data not shown) although the expression of specific PERK-eIF2α targets such as ATF4 were decreased (Fig. 5*A*). These results show that the shRNA-mediated down-regulation of PERK, although not dramatically affecting total protein synthesis and *in vitro* growth, is sufficient to down-regulate downstream targets of PERK (i.e., ATF4).

When inoculated *in vivo* on CAMs, D-HEp3 cells undergo on an average at most one population doubling, while, during the same time, the T-HEp3 cell population divided six to seven times (31). Therefore, D-control or D-shPERK nodules whose tumor cell count was >1 population doubling were scored as having escaped quiescence. We found that after 7 days *in vivo*, ~75% to 100% of the D-shPERK tumor nodules were able to proliferate, whereas only 20% of D-control nodules were able to do so (Fig. 5*B*). Moreover, D-shPERK tumors continued to expand upon serial passaging *in vivo*, whereas the D-control nodules failed to do so (data not shown). These results suggest that, in addition to its survival function, PERK has a functional role in the induction of growth arrest of D-HEp3 cells *in vivo*.

The high levels of PERK activity in D-HEp3 cells are insufficient to induce growth arrest in cell culture. This seemed to depend on the intensity of PERK signals as activation of Fv2E-PERK in D-HEp3 cells, which further enhances eIF2α phosphorylation, induces growth arrest in culture (Supplementary Fig. S2*D*). Whereas the basal p-eIF2α levels in D-HEp3 cells were ~2-fold higher than in T-HEp3 cells (Fig. 1*A* and *B*; ref. 23), the activation of Fv2E-PERK in T-HEp3 cells resulted in ~50-fold increase in p-eIF2α levels, which causes growth arrest both *in vitro* and *in vivo* (Fig. 2*B*). Thus, we examined whether a more controlled increase in p-eIF2α levels in T-Fv2E-PERK cells, comparable with that present basally in D-HEp3 cells, would suppress only the *in vivo* tumor growth. Treatment of T-Fv2E-PERK cells with 0.1 nmol/L AP20187 resulted in a moderate increase in p-eIF2α levels and, similar to D-HEp3 cells, did not induce a growth arrest *in vitro* (Fig. 5*C, inset*; data not shown). Twenty-four hours after treatment with this dose, the cells were inoculated and grown on CAMs for 4 days in the absence of AP20187 or with 0.0005 mg/kg of AP20187. Surprisingly, even these low levels of PERK activity were sufficient to inhibit tumor growth. Similar to D-HEp3 cells, these cells underwent around 1 population doubling, compared with 2 to 4 population doublings in untreated cells (Fig. 5*C*). Together, these results suggest that the high level of PERK in D-HEp3 cells is at a subthreshold level for inducing growth arrest *in vitro*, yet it contributes to the *in vivo* growth arrest program.

To further address the contribution of eIF2α phosphorylation to the *in vivo* arrest of D-HEp3 cells, we transiently overexpressed a FLAG-tagged GADD34 in D-HEp3 cells. Overexpression of GADD34 resulted in decreased eIF2α phosphorylation, which correlates with previously reported decrease in GADD153 promoter activity in these cells (Fig. 5*D, left*; ref. 23). Acute expression of GADD34 through transient transfection also resulted in a restoration of tumor growth (~5-fold; Fig. 5*D, right*). These results support the hypothesis that in D-HEp3 cells, activation of PERK and eIF2α phosphorylation in addition to signaling for survival (23) are also a part of the growth arrest program *in vivo*.

Discussion

We show here that tumor cells preserve the normal response to activated PERK-eIF2α signaling pathway by entering growth arrest while enhancing the survival response. The survival arm of this pathway in tumor cells has been previously documented (12, 13) and has led to the notion that targeting PERK activity might reduce tumor cell survival and thus benefit cancer patients (34–36). However, our results show that the growth arrest function of PERK found in normal cells (10, 37) is also operational in tumors. Therefore, the inhibition of PERK, through restoration of proliferative capacity, may exert a harmful effect because during natural cancer progression, regions of primary tumors, solitary disseminated tumor cells, as well as micrometastases, are in a slow dividing, or in a growth-arrested, dormant state (18–20).

Although high PERK activation promoted survival of the *in vivo* quiescent D-HEp3, in response to stress-induced apoptosis (23), whether it was functionally linked to the growth capacity of these cells *in vivo* was unknown. Genetic inhibition of PERK signaling in D-HEp3 cells restored the ability of these cells to grow *in vivo* by interrupting the G_0-G_1 arrest. In agreement, activation of this pathway in T-HEp3 or SW620 cells dramatically inhibited tumor growth *in vivo* by inducing growth arrest. Our studies show that the intensity of PERK signaling can induce a context-dependent (i.e., *in vitro* versus *in vivo*) growth arrest. The higher basal PERK signaling level does not affect D-HEp3 proliferation *in vitro*, a response that was also found when a comparable activation was achieved experimentally in T-Fv2E-PERK cells. However, this signal intensity was sufficient to inhibit tumor growth *in vivo*. This difference between the growth capacity of D-HEp3 cells *in vitro* and *in vivo* could be due to the cell culture conditions (high glucose, high oxygen tensions, etc.) that may override the growth inhibitory effects of the high PERK-eIF2α signaling. Of note is the fact that PERK inhibition never fully restored the proliferative capacity of D-HEp3 cells to the parental T-HEp3 levels (24 hours *in vivo* population doubling time), suggesting that it was not the only pathway regulating the growth arrest and that other signals (i.e., high p38, low epidermal growth factor receptor and ERK; ref. 31) might persist as growth-suppressive signals.

Fv2E-PERK–induced growth arrest in T-HEp3 cells was linked to decreased expressions of the G_1-S transition regulators cyclin D1, cyclin D3, and cyclin A, and negative Ki67 and pH3 staining. In NIH3T3 cells, PERK-mediated translation inhibition results in down-regulated cyclin D1 synthesis, which is crucial for UPR-induced cell cycle arrest (10, 37). It remains to be elucidated whether the same mechanism leads to cyclin D1 reduction following PERK activation in T- or D-HEp3 cells *in vivo*. PERK-mediated eIF2α phosphorylation results in a selective attenuation of translation. Thus, its tumor growth–suppressive effect is not merely the outcome of general protein synthesis inhibition, but rather the activation of a specific translation growth arrest program. This is evident from our observations that unlike cycD1 and cycD3, expression of p38, ERK, p53, and p21 are unaffected by the translation inhibition. Paradoxically, this translation inhibition also leads to the selective translational enhancement of several mRNAs necessary for survival and adaptation of cellular stress (9, 13, 38). Further studies using microarray analysis of polysome-bound mRNAs will help identify those genes selectively translated during PERK-dependent tumor growth inhibition.

Because the concept of dormancy or quiescence implies reversibility, it is important that the Fv2E-PERK–induced "dormancy-like" state in T-HEp3 cells *in vitro* was found to be reversible. This *in vitro* reversibility could be explained by the induction of GADD34 expression following Fv2E-PERK activation, as previously reported (39). *In vivo* studies showed that transient activation of Fv2E-PERK resulted only in a temporary inhibition of tumor growth *in vivo*. Similarly, activation of Fv2E-PERK with 3 mg/kg of dimerizer resulted in a reversible tumor growth arrest after ~30 days of treatment. However, Fv2E-PERK–induced growth arrest *in vivo* was not always reversible. For instance, we found that treatment of animals bearing T-Fv2E-PERK tumors with a higher dimerizer dose (5 mg/kg) resulted in irreversible growth suppression. The mechanism behind this irreversible arrest is unknown,

but it clearly depends on the intensity of PERK activation. Recent studies show that in normal melanocytes, induction of ATF6, ATF4, and XBP-1 activate senescence (in general, an irreversible arrest) in response to Ha-Ras signals (15). Further studies will determine whether an irreversible senescence-like program might be responsible for PERK-dependent tumor suppression *in vivo*. Other studies support that PERK activation or eIF2α phosphorylation in mammary epithelial cells or fibroblasts can inhibit tumor growth (14, 16, 17). Together, our studies support the conclusion that activation of PERK can engage a growth arrest program in tumors.

We would like to propose that targeting genes involved exclusively in the PERK-mediated survival program without affecting the growth arrest signals may be more attractive targets. Moreover, unlike PERK, activation/induction of other arms of the UPR (XBP-1, ATF-6, and BiP) do not seem to affect the proliferation machinery but are critical for the survival of tumor cells (21, 40–45). Therefore, inhibition of the survival function of PERK in combination with other prosurvival arms of the UPR such as XBP-1 might be an attractive therapeutic option.

Acknowledgments

Received 11/12/2007; revised 2/27/2008; accepted 3/10/2008.

Grant support: Samuel Waxman Cancer Research Foundation Tumor Dormancy Program (J.A. Aguirre-Ghiso and D. S. Conklin), NIH/National Cancer Institute grant CA109182 (J.A. Aguirre-Ghiso), and U.S. Army Medical Research Acquisition Activity grant W8IWXH-04-1-0474 (D.S. Conklin). A.C. Ranganathan is a recipient of a Ruth L. Kirschstein National Research Service Award (NIH/National Cancer Institute) Fellowship.

The costs of publication of this article were defrayed in part by the payment of page charges. This article must therefore be hereby marked *advertisement* in accordance with 18 U.S.C. Section 1734 solely to indicate this fact.

We thank Dr. David Ron (New York University, New York, NY) for providing the Fv2E-ΔNPERK and GADD34 constructs; Guy Russo (Center for Functional Genomics, University at Albany) for assisting us with plasmid preparations; Dr. Alejandro Adam and Bibiana Iglesias for help with the mice work and immunohistochemistry; Ariad Pharmaceuticals for AP20187 (http://www.ariad.com); and Dr. Liliana Ossowski (Mount Sinai School of Medicine) for critical reading of the manuscript.

References

1. Sonenberg N, Mathews, MB, Hershey JWB. Translational control of gene expression. New York: CSHL Press; 2000. p. 547–60.
2. Proud CG. eIF2 and the control of cell physiology. Semin Cell Dev Biol 2005;16:3–12.
3. Xu C, Bailly-Maitre B, Reed JC. Endoplasmic reticulum stress: cell life and death decisions. J Clin Invest 2005; 115:2656–64.
4. Yoshida H. ER stress and diseases. FEBS J 2007;274: 630–58.
5. Zhang K, Kaufman RJ. The unfolded protein response: a stress signaling pathway critical for health and disease. Neurology 2006;66:S102–9.
6. Zhao L, Ackerman SL. Endoplasmic reticulum stress in health and disease. Curr Opin Cell Biol 2006;18: 444–52.
7. Brewer JW, Hendershot LM, Sherr CJ, Diehl JA. Mammalian unfolded protein response inhibits cyclin D1 translation and cell-cycle progression. Proc Natl Acad Sci U S A 1999;96:8505–10.
8. Harding HP, Zhang Y, Zeng H, et al. An integrated stress response regulates amino acid metabolism and resistance to oxidative stress. Mol Cell 2003;11:619–33.
9. Harding HP, Novoa I, Zhang Y, et al. Regulated translation initiation controls stress-induced gene expression in mammalian cells. Mol Cell 2000;6: 1099–108.
10. Brewer JW, Diehl JA. PERK mediates cell-cycle exit during the mammalian unfolded protein response. Proc Natl Acad Sci U S A 2000;97:12625–30.
11. Harding HP, Zhang Y, Bertolotti A, Zeng H, Ron D. Perk is essential for translational regulation and cell survival during the unfolded protein response. Mol Cell 2000;5:897–904.
12. Bi M, Naczki C, Koritzinsky M, et al. ER stress-regulated translation increases tolerance to extreme hypoxia and promotes tumor growth. EMBO J 2005;24: 3470–81.
13. Blais JD, Addison CL, Edge R, et al. Perk-dependent translational regulation promotes tumor cell adaptation and angiogenesis in response to hypoxic stress. Mol Cell Biol 2006;26:9517–32.
14. Sequeira SJ, Ranganathan AC, Adam AP, Iglesias BV, Farias EF, Aguirre-Ghiso JA. Inhibition of proliferation by PERK regulates mammary acinar morphogenesis and tumor formation. PLoS ONE 2007;2:e615.
15. Denoyelle C, Abou-Rjaily G, Bezrookove V, et al. Anti-oncogenic role of the endoplasmic reticulum differentially activated by mutations in the MAPK pathway. Nat Cell Biol 2006;8:1053–63.
16. Donze O, Jagus R, Koromilas AE, Hershey JW, Sonenberg N. Abrogation of translation initiation factor eIF-2 phosphorylation causes malignant transformation of NIH 3T3 cells. EMBO J 1995;14:3828–34.
17. Perkins DJ, Barber GN. Defects in translational regulation mediated by the α subunit of eukaryotic initiation factor 2 inhibit antiviral activity and facilitate the malignant transformation of human fibroblasts. Mol Cell Biol 2004;24:2025–40.
18. Aguirre-Ghiso JA. Models, mechanisms and clinical evidence for cancer dormancy. Nat Rev Cancer 2007;7: 834–46.
19. Chambers AF, Groom AC, MacDonald IC. Dissemination and growth of cancer cells in metastatic sites. Nat Rev Cancer 2002;2:563–72.
20. Kufe D, Pollock RE, Weichselbaum RR, Bast RC, Jr., Gansler TS, Holland JF, Frei E III. Cancer medicine, 6th edition. Hamilton (Canada): BC Decker, Inc.; 2003. p. 161–94.
21. Aguirre-Ghiso JA, Ossowski L, Rosenbaum SK. Green fluorescent protein tagging of extracellular signal-regulated kinase and p38 pathways reveals novel dynamics of pathway activation during primary and metastatic growth. Cancer Res 2004;64:7336–45.
22. Ossowski L, Reich E. Changes in malignant phenotype of a human carcinoma conditioned by growth environment. Cell 1983;33:323–33.
23. Ranganathan AC, Zhang L, Adam AP, Aguirre-Ghiso JA. Functional coupling of p38-induced up-regulation of BiP and activation of RNA-dependent protein kinase-like endoplasmic reticulum kinase to drug resistance of dormant carcinoma cells. Cancer Res 2006;66:1702–11.
24. Goi T, Fujioka M, Satoh Y, et al. Angiogenesis and tumor proliferation/metastasis of human colorectal cancer cell line SW620 transfected with endocrine glands-derived-vascular endothelial growth factor, as a new angiogenic factor. Cancer Res 2004;64:1906–10.
25. De Haro C, Mendez R, Santoyo J. The eIF-2α kinases and the control of protein synthesis. FASEB J 1996;10: 1378–87.
26. Williams BR. PKR; a sentinel kinase for cellular stress. Oncogene 1999;18:6112–20.
27. Lu PD, Jousse C, Marciniak SJ, et al. Cytoprotection by pre-emptive conditional phosphorylation of translation initiation factor 2. EMBO J 2004;23:169–79.
28. Ma Y, Lu Y, Zeng H, Ron D, Mo W, Neubert TA. Characterization of phosphopeptides from protein digests using matrix-assisted laser desorption/ionization time-of-flight mass spectrometry and nanoelectrospray quadrupole time-of-flight mass spectrometry. Rapid Commun Mass Spectrom 2001;15:1693–700.
29. Su Q, Wang S, Gao HQ, et al. Modulation of the eukaryotic initiation factor 2 α-subunit kinase PERK by tyrosine phosphorylation. J Biol Chem 2008;283: 469–75.
30. Ossowski L. *In vivo* invasion of modified chorioallantoic membrane by tumor cells: the role of cell surface-bound urokinase. J Cell Biol 1988;107:2437–45.
31. Aguirre Ghiso JA, Kovalski K, Ossowski L. Tumor dormancy induced by downregulation of urokinase receptor in human carcinoma involves integrin and MAPK signaling. J Cell Biol 1999;147:89–104.
32. Hewitt RE, McMarlin A, Kleiner D, et al. Validation of a model of colon cancer progression. J Pathol 2000;192: 446–54.
33. Parle-McDermott A, McWilliam P, Tighe O, Dunican D, Croke DT. Serial analysis of gene expression identifies putative metastasis-associated transcripts in colon tumour cell lines. Br J Cancer 2000;83:725–8.
34. Feldman DE, Chauhan V, Koong AC. The unfolded protein response: a novel component of the hypoxic stress response in tumors. Mol Cancer Res 2005;3: 597–605.
35. Fels DR, Koumenis C. The PERK/eIF2α/ATF4 module of the UPR in hypoxia resistance and tumor growth. Cancer Biol Ther 2006;5:723–8.
36. Koumenis C. ER stress, hypoxia tolerance and tumor progression. Curr Mol Med 2006;6:55–69.
37. Brewer JW, Cleveland JL, Hendershot LM. A pathway distinct from the mammalian unfolded protein response regulates expression of endoplasmic reticulum chaperones in non-stressed cells. EMBO J 1997;16:7207–16.
38. Blais JD, Filipenko V, Bi M, et al. Activating transcription factor 4 is translationally regulated by hypoxic stress. Mol Cell Biol 2004;24:7469–82.
39. Novoa I, Zeng H, Harding HP, Ron D. Feedback inhibition of the unfolded protein response by GADD34-mediated dephosphorylation of eIF2α. J Cell Biol 2001; 153:1011–22.
40. Carrasco DR, Sukhdeo K, Protopopova M, et al. The differentiation and stress response factor XBP-1 drives multiple myeloma pathogenesis. Cancer Cell 2007;11: 349–60.
41. Koong AC, Chauhan V, Romero-Ramirez L. Targeting XBP-1 as a novel anti-cancer strategy. Cancer Biol Ther 2006;5:756–9.
42. Lee AS. GRP78 induction in cancer: therapeutic and prognostic implications. Cancer Res 2007;67:3496–9.
43. Ranganathan AC, Adam AP, Zhang L, Aguirre-Ghiso JA. Tumor cell dormancy induced by p38SAPK and ER-stress signaling: an adaptive advantage for metastatic cells? Cancer Biol Ther 2006;5:729–35.
44. Romero-Ramirez L, Cao H, Nelson D, et al. XBP1 is essential for survival under hypoxic conditions and is required for tumor growth. Cancer Res 2004;64:5943–7.
45. Shuda M, Kondoh N, Imazeki N, et al. Activation of the ATF6, XBP1 and grp78 genes in human hepatocellular carcinoma: a possible involvement of the ER stress pathway in hepatocarcinogenesis. J Hepatol 2003;38: 605–14.